Engineering

Measuring the Time-evolution of Nanoscale Materials with Stopped-flow and Small-angle Neutron Scattering

Published: August 6, 2021 doi: 10.3791/62873

Elizabeth G. Kelley[1], Michael H. L. Nguyen[2], Drew Marquardt[2,3], Brian B. Maranville[1], Ryan P. Murphy[1]

[1]NIST Center for Neutron Research, **National Institute of Standards and Technology**, [2]Department of Chemistry and Biochemistry, **University of Windsor**, [3]Department of Physics, **University of Windsor**

Abstract

This paper presents the use of a stopped-flow small-angle neutron-scattering (SANS) sample environment to quickly mix liquid samples and study nanoscale kinetic processes on time scales of seconds to minutes. The stopped-flow sample environment uses commercially available syringe pumps to mix the desired volumes of liquid samples that are then injected through a dynamic mixer into a quartz glass cell in approximately 1 s. Time-resolved SANS data acquisition is synced with the sample mixing to follow the evolution of the nanostructure in solution after mixing.

To make the most efficient use of neutron beam time, we use a series of flow selector valves

throughout multiple sample injections. Sample injections are repeated until sufficient

Introduction

concentrations, additive concentrations, and temperatures. The minimum sample volume required per injection is approximately 150 µL depending on the path length of the quartz cell.

Representative results using this stopped-flow sample environment are presented for rapid lipid exchange kinetics in the presence of an additive, cyclodextrin. The vesicles exchange outer-leaflet (exterior) lipids on the order of seconds and fully exchange both interior and exterior lipids within hours. Measuring lipid exchange kinetics requires *in situ* mixing to capture the faster (seconds) and slower (minutes) processes and extract the kinetic rate constants. The same sample environment can also be used to probe molecular exchange in other types of liquid samples such as lipid nanoparticles, proteins, surfactants, polymers, emulsions, or inorganic nanoparticles. Measuring the nanoscale structural transformations and kinetics of exchanging or reacting systems will provide new insights into processes that evolve at the nanoscale.

Introduction

Small-angle neutron scattering (SANS) provides a unique way to measure the sizes, shapes, interactions, and organization of various materials on length scales from ≈1 nm to ≈100 nm[1,2,3]. Recent instruments, including VSANS (very small-angle neutron scattering) instruments with focusing mirrors, push the limits toward measuring even larger length scales up to ≈1000 nm[4,5]. In general, the unique scattering contrast inherent to neutron scattering methods offers several advantages in measuring the time-evolution of nanoscale structures, such as the aggregatio components in pharmaceutical formulations[6], crosslinking and gelation reactions in polymer

View Video

[1,12], and growth of silica-based materials[13,14,15]. The unique scattering contrast makes

Introduction

Stopped-flow mixing methods often are implemented in small-angle X-ray scattering (SAXS)[16,17,18,19,20,21], fluorescence spectroscopy[22,23,24,25,26], and light scattering[27,28,29,30,31,32] experiments to study kinetic processes on the millisecond time scales. An important difference between SANS and SAXS is that neutron scattering is a nondestructive characterization technique, and as such, SANS can be used to measure the same sample for hours or even days without ionizing radiation damage to the sample, which can happen during higher-flux X-ray scattering experiments[33]. As repeated SANS measurements will not alter the chemical structure of the probe molecule or sample, the time-evolution can be studied without effects of photobleaching, for example, which can complicate kinetics measurements that rely on fluorescence[23,24]. Moreover, SANS can be used to measure highly concentrated and optically opaque samples that are often difficult to characterize with light-based techniques such as dynamic light scattering.

In addition to providing structural information on the nanoscale, SANS can be used to probe the local composition of these structures through the variation in neutron scattering length density contrast. The scattering length density (SLD) of different elements varies randomly across the periodic table and varies with different isotopes of the same element. A commonly exploited example is hydrogen (^{1}H or H) and deuterium (^{2}H or D), which have vastly different neutron scattering lengths. Therefore, hydrogen-rich materials, such as surfactants, lipids, proteins, RNA, DNA, and other polymers, can be distinguished from deuterated solvents using SANS without

View Video

ange can affect the density, hydrogen-bonding, and phase transition temperatures in

Introduction

signal in X-ray based techniques such as SAXS. Isotopic substitution also makes SANS a powerful tool for studying molecular exchange kinetics in hydrogen-rich materials by simply mixing H-labeled and D-labeled molecules. Isotopic substitution is particularly useful in systems where bulky fluorescent dyes are larger than the surfactant or lipid molecules of interest and can influence the exchange kinetics[34,35].

Time-resolved SANS measurements are advantageous because the measured intensity is a function of time, length scale, and SLD contrast. As such, TR-SANS experiments can be designed to probe the time-dependent changes in the spatial distributions and the compositions of the samples. These unique advantages of SANS have led to important insights into kinetic processes in many soft material systems such as surfactants[36,37,38], emulsions[39,40,41], lipids[34,42,43,44,45,46,47,48,49,50], and polymers[51,52,53,54,55,56,57,58,59,60,61,62]. Most TR-SANS studies have focused on time scales of minutes to hours. However, many kinetic processes of interest occur on the second time scale and are essential for understanding the underlying mechanisms. Capturing these early time points requires that the solutions be rapidly mixed and measured *in situ*, in which the mixing is synced with data collection during stopped-flow light scattering[27,28,29,30,31,32], fluorescence[22,23,24,25,26], and X-ray[16,17,18,19,20,21] experiments. This work describes the use of a sample environment designed to rapidly mix multiple liquid samples and inject the mixture into a quartz glass cell for TR-SANS measurements. The mixing device is an adaptation of the recently developed capillary rheoSANS device[63] and uses multiple syringe pumps and valves to control the sample mixing and to automate cell cleaning. By connecting

View Video

easured, rinsed, and dried to facilitate TR-SANS measurements on the seconds time

Introduction

We focus on the *in situ* mixing setup and methods to collect TR-SANS data. Neutron scattering data were collected on the VSANS instrument at the NIST Center for Neutron Research (NCNR); however, the procedure should be applicable to other SANS instruments. Readers interested in implementing similar protocols on other SANS instruments should consult with the local instrument scientists to determine the optimal instrument configuration to maximize neutron flux at the desired length scale and time scale most relevant to the kinetic processes of interest. The data presented here were collected using the high flux 'white beam' configuration on VSANS to maximize neutron counts at the loss of spatial resolution[5]. The detector carriages were positioned to cover a range of scattering vectors (q), 0.005 $Å^{-1}$ < q < 0.5 $Å^{-1}$, corresponding to length scales of ≈130 nm to ≈13 nm. The scattering vector is defined as $q = 4\pi/\lambda \sin(\theta/2)$ in which λ is the neutron wavelength, and θ is the scattering angle.

The stopped-flow mixing device used for the TR-SANS measurements consists of multiple pumps, rinsing syringes, sample syringes, flow selectors, as well as adynamic mixer, sample cell, and mixed sample container, as shown in **Figure 1**. All sealed fluid paths are located inside an air-conditioned enclosure, which includes the syringes, valves, connection tubing, dynamic mixer, and sample cells. A programmable thermoelectric air conditioner is used to control the enclosure temperature in the range from 10 °C to 50 °C within ±1 °C. Note that some of the enclosure insulation was removed to show the working parts of the device. The main mixing device enclosure is positioned on a translational stage on the NG3 VSANS beam line at the

View Video

ıe enclosure position is adjusted using the translation stage to position the sample cell

Introduction

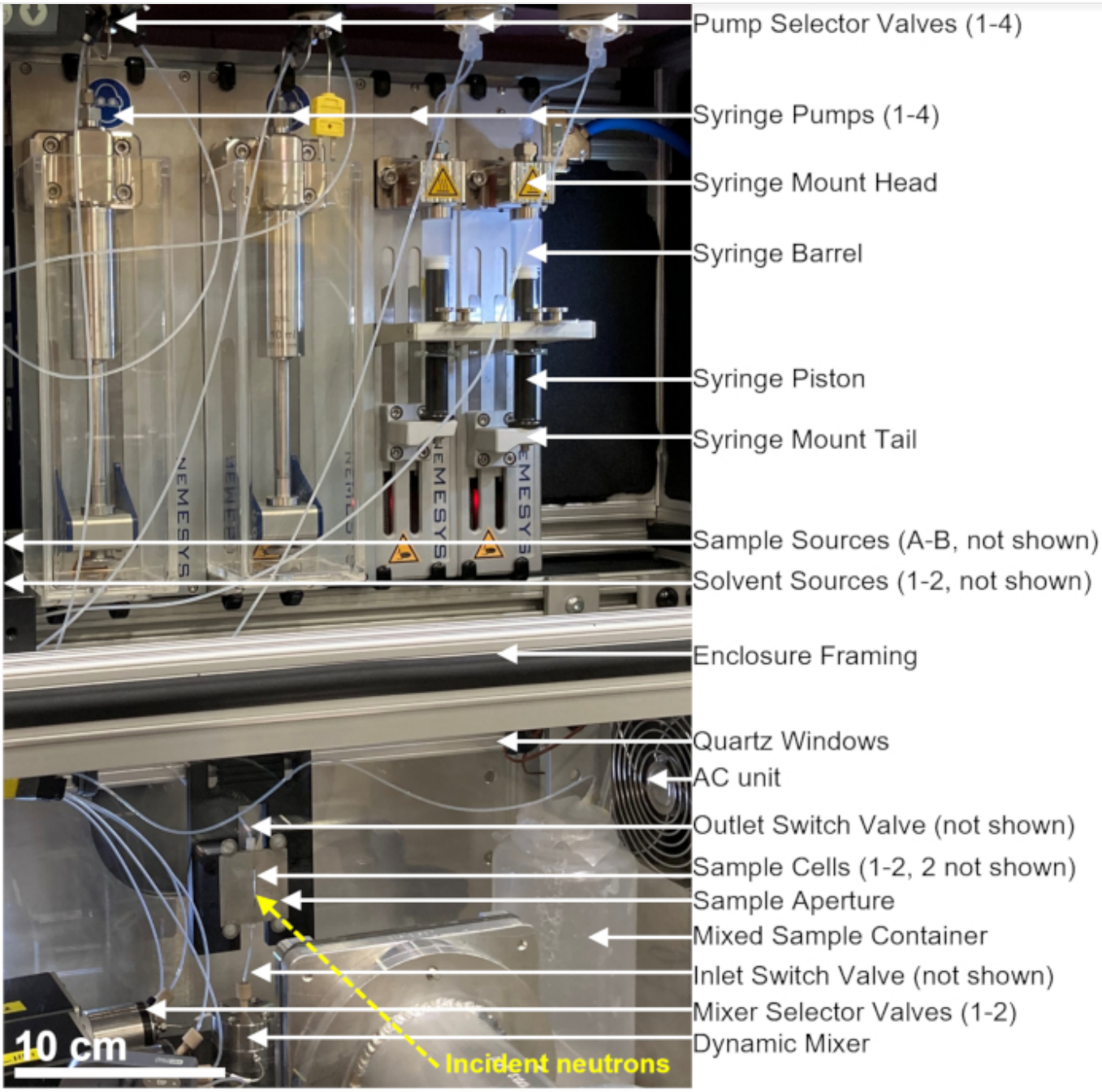

Figure 1: An example setup for combining stopped-flow mixing and small-angle neutron scattering measurements at the VSANS beamline at the NIST Center for Neutron

View Video

for sample injection, four pump selector valves, two mixer selector valves, a dynamic

Introduction

thermoelectric air-conditioned unit is used to control the sample and all equipment at a constant temperature. The yellow dashed line shows the neutron beam path. Scale bar = 10 cm. **Please click here to view a larger version of this figure.**

The device depicted in **Figure 1** is configured with two sample syringes, two rinsing syringes, and one sample cell. Corresponding flow diagrams for the different steps of the protocol are illustrated in **Figure 2**. The desired volumes of the two different samples are injected into the mixer and the sample cell (**Figure 2A**). Once the sample cell is filled, the Inlet Switch Valve (ISV) and Outlet Switch Valve (OSV) are closed to isolate the sample cell from the dynamic mixer and to prevent sample back diffusion into the cell during TR-SANS data collection (**Figure 2B**). Before the dynamic mixer, the connection tubing varies in length from 10 cm to 1 m and does not affect the mixing delay time. However, tubing connections between the dynamic mixer and the sample cell will affect the mixing delay time and the required sample injection volume. Precut stainless steel tubing with 0.04 inch (1 mm) inner diameter and 100 mm length are used to connect the dynamic mixer, the Mixer Selector Valves (MSV1 and MSV2), and the ISV and OSV. Fluorinated tubing with 1 mm inner diameter and 115 mm length is used to connect the ISV and OSV (or the dynamic mixer outlet) to the sample cell. The total void volume that influences the mixing delay time includes the mixer void volume (0.15 mL), the tubing between the mixer outlet and the sample cell inlet (0.09 mL), and the sample cell volume (0.16 mL). In this example, the total void volume is 0.4 mL. The internal void volumes of valves are negligible compared the tubing, mixer, and sample cell void volumes. For example, the employed low-pressure

View Video

sure selector valves and switch valves (0.25 mm bore diameter) contain approximate

Introduction

and rinse solvent is repeatedly pumped through the cell to remove the residual sample and clean the sample cell (**Figure 2C**). Note that the rinse syringes are connected to larger solvent reservoirs (e.g., water and ethanol) via pump selector values to ensure that adequate solvent volumes are available to clean the sample cell between measurement runs. Solvent sources, sample sources, and mixed sample containers that contain flammable liquids are positioned in a separate enclosure with no electrical equipment to eliminate all possible ignition sources. In addition, vapor-locking bottle caps are used to minimize flammable vapors and solvent evaporation. Finally, the sample cell is dried with a nitrogen gas stream to remove the residual rinse solvent (**Figure 2D**). The inlet nitrogen gas pressure to the mixer selector valve is regulated to approximately 2 bar (0.2 MPa, gauge pressure) using a manual pressure regulator located on the nitrogen gas cylinder. Once the sample cell is sufficiently cleaned and dried, a newly mixed sample is injected into the sample cell for the next measurement cycle (repeating the mixing and injection illustrated in the flow diagram in **Figure 2A**).

Introduction

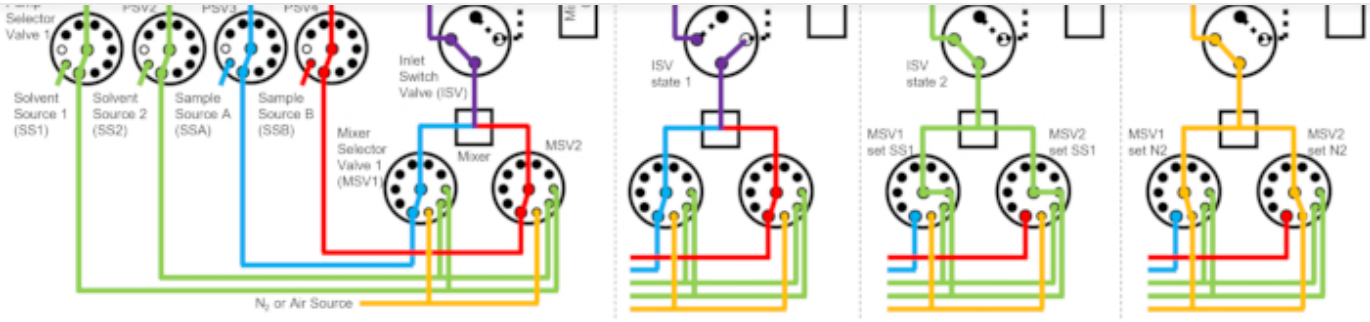

Figure 2: Example flow diagram using one sample cell, two samples mixing, and two rinse solvents for cleaning. (**A**) Mixing of sample A (blue) and sample B (red), and then flowing the mixed sample (purple) into the sample cell. (**B**) During data collection, the stopped-flow device state where the ISV and OSV switch valves are closed to isolate the sample cell and prevent back diffusion of the sample during data collection. (**C**) The cleaning steps where the sample cell is rinsed with rinse solvent from SS1 (green) after data collection. (**D**) Drying step where the sample cell is dried with nitrogen gas (orange). Abbreviations: PSV = pump selector valve; MSV = mixer selector valve; OSV = outlet switch valve; ISV = inlet switch valve; SS1 = solvent source 1; SSA = sample source A; N2 = nitrogen gas source. **Please click here to view a larger version of this figure.**

Figure 3 shows flow diagrams for a slightly different version in which the mixing setup is configured with two separate sample cells connected to the same switch valves (**Figure 3A**). While TR-SANS data are collected in Sample Cell 1, Sample Cell 2 is rinsed (**Figure 3B**) and dried (**Figure 3C**). When the data collection is complete for Sample Cell 1, the Inlet Switch Valve directs a newly mixed sample into Sample Cell 2 for data collection (**Figure 3D**). While TR-SANS

View Video

collected in Sample Cell 2, Sample Cell 1 is rinsed and dried (**Figure 3E**). This

Introduction

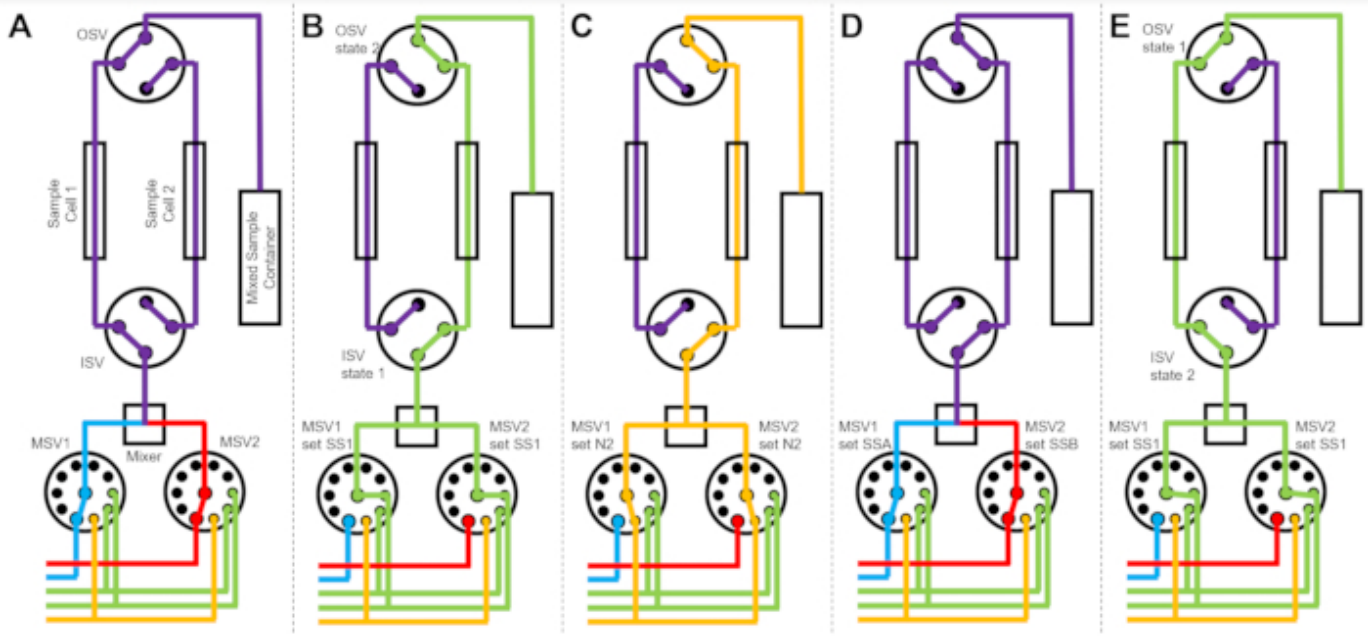

Figure 3: Example flow diagram using a two-sample cells, two samples mixing, and two rinse solvents for cleaning. (**A**) Mixing sample A (blue) and sample B (red) and then flowing the mixed sample (purple) into sample cell 1. (**B**) The stopped-flow device state during data collection on sample cell 1 while sample cell 2 is rinsed with solvent from SS1 (green). (**C**) The stopped-flow device state during data collection on sample cell 1 while sample cell 2 is dried with nitrogen gas (orange). (**D**) Once data collection of sample cell 1 is complete, a new sample (purple) is immediately mixed and flowed into sample cell 2. (**E**) The stopped-flow device state during data collection on sample cell 2 while sample cell 1 is rinsed with solvent from SS1 (green). While one sample cell is being measured, the other sample cell is being cleaned and dried. The stopped-flow measurement process alternates between two sample cells to mini the time between subsequent sample mixing injections. Abbreviations: PSV = pump selector

View Video

ɔurce 1; SSA = sample source A; N2 = nitrogen gas source. **Please click here to view a**

the system, rinsing and drying the sample cell, and injecting the mixed sample. Although the single-cell configuration is demonstrated for simplicity (**Figure 2**), the flexible modular setup, protocol, and scripts can be easily modified to implement more syringe pumps, valves, mixers, or sample cell configurations, such as the two-sample cell configuration shown in **Figure 3**. Representative raw neutron count rate data collected throughout mixing and cleaning injection cycles are shown in **Figure 4**, while lipid exchange kinetics measured at 3 different temperatures and the extracted normalized scattered intensity corresponding to the fraction of lipids exchanged are shown in **Figure 5** and **Figure 6**, respectively.

Protocol

1. Set up and initiate the stopped-flow system.

1. Turn on all pump power supplies and dynamic mixers using the power switch.
2. Initiate all pumps and valves in the stopped-flow system control graphical user interface (GUI) by entering the device configuration path and using the commands **bus=qmixbus.Bus()**, **bus.open()**, **bus.start()**, **pump=qmixpump.Pump()**, **pump.enable()**, and **valve=ViciMultiposSelector()** (see example initiation code available in an online open-source repository[64]).
3. Calibrate the pumps before attaching syringes using the command **pump.calibrate()**.
4. Confirm that the valves are initiated and move to the correct selector port on command using the command **valve.setPort()** and **valve.getPort()**.
5. Assign the syringe type to be used for each pump using the command

View Video

ıe syringe max piston stroke distance (mm).

Introduction

2. When using glass syringes, ensure the syringe mount head is loosened before dispensing the fill volume, so that the glass syringe does not break due to excessive force from the syringe piston.
3. Screw in the syringe piston to the connection at the bottom of the pump (syringe mount tail).
4. After the syringe barrel and syringe piston are connected to the pump, dispense the fill volume of the syringe type using the command **pump.empty()**, which moves the syringe piston to the top of the syringe barrel.
5. When using glass syringes, tighten the syringe mount head after the piston movement stops.

7. Connect the tubing to the sample and solvent sources, syringes, valves, mixers, sample cells, and mixed sample container.
    1. Connect the syringe pump tubing to the pump selector valves.
    2. Connect the pump selector valve tubing to the sample sources.
    3. Connect the pump selector valve tubing to the rinsing solvent sources.
    4. Connect the pump selector valve tubing to the mixer selector valve tubing.
    5. Connect the mixer selector valve tubing to the nitrogen gas source.
    6. Connect the mixer selector valve tubing to the mixer inlets.
    7. Connect the mixer outlet to the inlet switch valve.
    8. Connect the inlet switch valve to the sample cell inlet.
    9. Connect the sample cell outlet to the outlet switch valve.
    10. Connect the outlet switch valve to the mixed sample container.
8. Define all tubing and valve connections made (Step 1.7) in the stopped-flow system cont...

View Video

mple control code in the online open-source repository[64]).

Introduction

2. Load the sample.

1. Set the desired sample fill volume and solvent fill volume in the stopped-flow system control GUI by typing the desired numbers (see example control code in the online open-source repository[64]).
2. Use the **pump.aspirate()** command to pull in (aspirate) the desired sample and solvent volumes from their sources into the sample syringes through the pump selector valves.
   NOTE: When first loading an empty syringe, air will be present at the top of the syringe that must be purged to prime the system with sample and solvent in step 3.

3. Prime the system.

1. Use the **pump.dispense()** command to push out (dispense) all air from syringes, tubing lines, and valves. Ensure that enough liquid volume is dispensed from each syringe to completely remove all air from the syringes, tubing, and valves. If air bubbles are visible inside any tubing, continue dispensing solvent or sample until the bubbles are removed.
2. Once air has been purged from the system, perform at least one sample injection and rinsing procedure (without neutron scattering data collected).
    1. Click to select the cell labeled **Start mixing experiment** in the control GUI.
    2. With this cell actively selected, click on the **Run** button (right triangle) located at the top of the control GUI, or press the **Shift** and **Enter** keys together on the keyboard.
    3. Visually inspect the sample cell to confirm that air bubbles are not present.
        1. If air bubbles are present, repeat protocol steps 3.1 and 3.2 to further purge air from the tubing lines.

View Video

2. If air bubbles are not present in the sample cell, proceed to step 4 to define the

Introduction

the online open source repository).

1. Enter the temperature set point of the programmable air conditioner (AC) unit that controls the temperature of the insulated enclosure surrounding the stopped-flow device.
    1. While holding the **star** button on the AC control unit, press the **up** and **down** arrows to change the setpoint temperature. Alternatively, type the desired temperature setpoint in the control GUI and click on **Run**.
    2. Wait for 15-30 min to allow the enclosure interior to equilibrate at the desired temperature before starting the kinetic experiments.

       NOTE: The accessible temperature range is currently between 10 °C and 50 °C, and the temperature stability is ± 1 °C.
2. Enter all rinsing sequence steps by typing in the appropriate volumes, flow rates, times, and number of repetitions into the control GUI.
    1. Define the volume of each sample to be injected, which defines the total flow rate (Q).
    2. Define the volume of each solvent to be injected during the rinsing procedure.
    3. Define the drying time between each rinsing substep (t_{dry}).
    4. Define the number of rinsing substeps.
    5. Define the different solvents for the subsequent rinsing steps.
    6. Define the number of rinsing repetitions to perform after each measurement (n_{rinse}).
    7. Define the time to fully dry the sample cell and mixer, providing a clean sample cell for the subsequent sample injection (t_{dry_final}).
3. Define all sample injection sequence steps by typing the appropriate volumes, flow rates, and times into the stopped-flow system control GUI.
    1. Define the volume of each sample to be injected and the flow rate.

View Video

2. Calculate the delay time (t_{delay}) from the void volume (V_{void}) and the total flow rate

3. Define the desired acquisition time for the TR-SANS data such that the entire kinetic process of interest has occurred (t_{scatt}).
4. Set the wait time between the end of the scattering experiment and the beginning of the rinse cycles (t_{wait}).

   NOTE: This wait time should be at least 100 s if the sample neutron transmission is to be measured before it is rinsed from the cell. The sample transmission is needed during data processing to reduce the data to absolute intensity.
5. Define the number of injection cycles to perform with rinsing sequences run between each injection that are defined in step 4.2 (n_{cycle}).

4. Calculate the total time of a single stopped-flow data collection cycle (t_{cycle}) using equation (**1**).

   $t_{cycle} = n_{rinse} \times (t_{delay} + t_{dry}) + t_{dry\_final} + t_{delay} + t_{scatt}$ (**1**)

   in which n_{rinse} = number of rinsing repetitions (step 4.2.6); t_{delay} = delay time of the stopped flow device (step 4.3.2); t_{dry} = drying time between each rinsing substeps (step 4.2.3); t_{dry_final} = time to fully dry the sample cell and mixer (step 4.2.7); t_{scatt} = desired TR-SANS data acquisition time (step 4.3.3)

5. Define the small-angle neutron scattering parameters in the SANS instrument control GUI.

1. Determine the length scales and q-range of interest for each sample.
2. Define the instrument configuration to cover the desired q-range of interest, while maximizing the neutron flux at the sample.
3. Set the total VSANS data acquisition time in the SANS instrument control GUI to the

the sample transmission measurement time to 100 s in the SANS instrument control

Introduction

6. Collect standard scattering measurements for data reduction before beginning the stopped-flow experiment to process the TR-SANS data.

1. Measure the background scattering.
    1. Ensure that the local instrument shutter is closed.
    2. Attach the blocked beam sample to the back of the sample aperture, secure the local instrument environment, and open the local instrument shutter.
    3. Define the blocked beam scattering data acquisition time in the software, and collect blocked beam scattering data, counting for the same duration as the longest scattering data acquisition time (t_{scatt}).
    4. Once the data collection is complete, close the instrument shutter, and remove the blocked beam sample from the sample aperture.
2. Measure the empty cell scattering.
    1. Ensure that the sample cell has been thoroughly rinsed and dried.
    2. Open the local instrument shutter.
    3. Collect the empty cell transmission measurement for 100 s.
    4. Collect the empty cell scattering measurement, counting for at least the longest acquisition time (t_{scatt}).

7. Begin the stopped-flow experiment.

1. Start VSANS scattering data collection in **event** mode.
    1. Ensure that the local instrument area is secure and then open the local instrume beam shutter.

View Video

2. Begin SANS data collection using the SANS instrument control software on the

before starting the stopped-flow mixing experiment. The data will be post-processed at a later step to account for the delay time (t_{delay}).

2. Start the stopped-flow mixing experiment in the control GUI.
    1. Select the notebook cell labeled **Start mixing experiment** in the stopped-flow system control GUI.
    2. With this cell actively selected, click on the **Run** button (right triangle) located at the top of the stopped-flow device control program, or press the **Shift** and **Enter** keys together on the keyboard.
    3. Confirm that the stopped-flow mixing protocol defined in section 4 has started operating.
    4. Add the 100 s transmission measurement to the VSANS instrument queue after the scattering run using the SANS instrument control GUI.
    5. Add one scattering measurement run and one transmission measurement run to the instrument queue for each remaining stopped-flow mixing cycle (n_{cycle} - 1, step 4.3.5) in the SANS instrument control GUI.

8. Process and reduce data to remove all backgrounds, correct for detector sensitivity, and correct for sample transmission.

1. Download the scattering data files and associated event files from the server.

    NOTE: Separate detector event files will be generated after each VSANS measurement, one event file for each active detector carriage (e.g., front, middle, and/or back detector).
2. Bin the scattering data to desired time bins using the command **events=Rebin(filenam** followed by the command e**vents.do_rebinning(timebins)**, in which the input **filename**

View Video

e bin boundaries in seconds.

repository[64]).

3. Reduce the binned scattering data using the software provided the beamline[65].

9. Analyze the TR-SANS data.

1. Calculate the process time of interest ($t_{process}$) from the measurement times using equation (**2**).

   $t_{process} = t_i - t_{stop} + t_{delay}$ (**2**)

   Where t_i is the measurement time bins starting after the flow is stopped, t_{stop} is the measurement time immediately when the flow is stopped, and t_{delay} is the delay time.
2. Plot the q-dependent intensity I(q) as a function of the process time using the time bins defined in step 8.2 and the $t_{process}$ calculated in step 9.1.

   NOTE: The earliest accessible process time is restricted by t_{delay}. To measure earlier process time points, increase the total flow rate (Q) or decrease the total void volume (V_{void}).
3. Extract the kinetic parameters of interest from the change in I(q) as a function of process time.

10. End the experiment.

1. Turn off the neutron beam by closing the local instrument shutter.
2. Perform a radiation check using a radiation monitor provided by the beamline before disconnecting any parts, tubing, or unloading any samples or mixed sample containers.
3. Transfer the syringes, tubing, and mixed sample container to the health physics department.

View Video

Introduction

with the exchange rate (k_e)[66,67]. Previous fluorescence studies have shown that k_e depends on the mβCD concentration, and the half-life of the exchange process is on the order of minutes[68]. The present experiments use stopped-flow TR-SANS to measure mβCD-catalyzed lipid exchange between vesicles on the seconds time scale. Two isotopically distinct lipid vesicle populations were prepared; one vesicle population was prepared with tail-hydrogenated dimyristoylphosphatidylcholine (DMPC) lipids (H-lipid vesicles in **Figure 5**), and the other vesicle population was prepared with tail-deuterated DMPC (DMPC-d54) lipids (D-lipid vesicles in **Figure 5**). A mole fraction of 0.05 (5 mol%) of charged dimyrisotylphosphatidylglyercol (DMPG) lipid was added to both the DMPC and DMPC-d54 dry lipid powders to promote unilamellar vesicle formation[69].

Separate H-vesicle and D-vesicle solutions were prepared by hydrating the respective lipid films in a solvent containing 45% by volume heavy water (D_2O) and 55% by volume water (H_2O). The D_2O/H_2O solvent composition was calculated such that the neutron scattering length density (ρ) of the solvent matched a random mixture of the H-lipids and D-lipids ($\Delta\rho = \rho_{lipid} - \rho_{solvent} = 0$). In other words, a randomly mixed H/D-vesicle would be 'invisible' to the neutrons and generate zero coherent neutron scattering. Unilamellar vesicle solutions were prepared by freeze-thawing the solutions five times and then extruding the individual solutions through a polycarbonate filter with 100 nm diameter pores. The vesicle solutions were extruded back and forth between two syringes and the filter for a total of 31 times at 30 °C. Subsequently, a small volume of a

View Video

e solutions. The final lipid concentration was 14 mmol/L (mM) and the mβCD

Introduction

flow mixing device.

An example of the measured neutron count rates over multiple injection cycles is shown in **Figure 4A**. Each cycle consisted of 9 rinsing steps, 1 drying step, and 1 sample injection step. Only count rates measured on the middle detector carriage in the VSANS instrument are presented for clarity. Similar trends were found on the front detector carriage, which corresponded to data collected at larger scattering angles or higher q values. The count rate spiked with each rinsing solvent injection (solvent S1 and solvent S2) and returned to the empty cell baseline counts when the solvent was pushed out of the cell with nitrogen gas and dried. The final cell rinse was with S2, which was ethanol in this example, and the cell was dried a final time with nitrogen gas for 3 min before sample injection. Soon after the sample was injected into the cell, the neutron count rate spiked, and data were collected continuously for 5 min. The representative sample injected in the example data in **Figure 4A** was a salt buffer background. The fluctuations in measured intensity over time reflect the variations in the background neutron count rate and do not reflect a change in the average sample composition. The complete cycle of rinsing, drying, mixing, and injecting sample was repeated an additional time in the example in **Figure 4A**, where each cycle lasted for a total of 15 min.

The individual H-labeled and D-labeled lipid vesicle solutions were mixed at time t_{mix} and immediately flowed into the sample cell. The measured neutron count rate spiked and then reached a maximum value when the sample cell was filled at t_{fill}, as shown in **Figure 4B**. The

View Video

: the void volume (V_{void}) between the mixer and the sample cell is known and the total

Introduction

leave the sample cell. After reaching t_{fill}, the flow was continued at a constant flow rate to ensure that the cell had filled and reached steady-state. The flow was then immediately stopped at t_{stop}. The averaged neutron count rate remained constant as a function of measurement time between t_{fill} and t_{stop} because the flow rate through the sample cell was constant, and therefore, the sample within the neutron beam path was at steady-state. In other words, the data measured at t_{stop} correspond to the sample that has been mixed and evolved by $t_{delay} = t_{fill} - t_{mix} = V_{void}/Q$. The binned measurement times t_i collected immediately after t_{stop} are the main kinetic data of interest.

In **Figure 4C**, the neutron counts from the mixed lipid vesicles sample at three different temperatures are plotted as a function of the corrected process time scale ($t_{process}$), which is the process time of interest that has been corrected for the steady-state flow period and delay time. The process time scale was calculated by $t_{process} = t_i - t_{stop} + t_{delay}$, or equivalently, $t_{process} = t_i - t_{stop} + t_{fill} - t_{mix}$. SANS data were collected continuously in **Figure 4** in so-called **event mode**. During **event mode** data collection, each detected neutron event is recorded with a unique time stamp and its x and y location on the two-dimensional neutron detector. Event mode data is then post-processed into the desired time bins (t_i) in **Figure 4B**.

Event mode data within the accessible process time window of interest (*i.e.*, neutron scattering collected at each t_i after t_{stop} in **Figure 4B**) were reconstructed into a two-dimensional (2D) detector image for that time bin using protocols and scripts available in the online open-sou

View Video

he different sources of background, correct for the sample transmission and detector

Introduction

the time- and length-scale dependent information that can be gained from a TR-SANS measurement. Similar to the total raw count rate shown in **Figure 4B**, the q-dependent intensity I(q) decreases in time as the lipids in the outer leaflet exchange and mix randomly between different vesicles.

Data are presented in **Figure 5** for the lipid exchange kinetics measured at 3 different temperatures. Each plot shows the data collected for the first 110 min after mixing. The measured intensity decreases by an order of magnitude at the lowest q-values at 36 °C and 30 °C, which correspond to the lipid fluid phase. Meanwhile, the scattered intensity data change significantly slower with time at 20 °C, indicating that the outer leaflet exchange kinetics are much slower in the lipid gel phase.

The measured scattering intensity, I(*q*), is related to the SLD contrast as $\sqrt{I(q)} \propto \Delta\rho$, in which Δρ is the SLD difference between the vesicle and the surrounding solvent. This average SLD contrast is directly related to the relative numbers of H-lipids and D-lipids in a vesicle at any given time. As such, the measured scattering intensity at a given time can be normalized to determine the fraction of the lipid population that has exchanged. This normalization is achieved by collecting two additional measurements, including: (1) the measured intensity I(0) at time t = 0, when there is no lipid exchange between vesicles, and (2) the measured intensity *I*(∞) at time t = ∞, when all of the lipids have exchanged and the populations have equilibrated. The normalized count rate, $R(t) = \left[\sqrt{I(t)} - \sqrt{I(\infty)}\right] / \left[\sqrt{I(0)} - \sqrt{I(\infty)}\right]$ [42], is plotted as a function of the process

View Video

ime t (background-subtracted intensity integrated as a function of q), I(∞) is the *q*-

Introduction

exchange). I(0) was measured for a mixed sample below the phase transition temperature at 20 °C where the exchange was slow, and I(∞) was measured in a separate sample that had equilibrated for more than 36 h at 40 °C and had and fully exchanged H-lipids and D-lipids.

The normalized count rate should decay from R(t) = 1 at process time t = 0, to R(t) = 0 at t = ∞, and is directly related to SLD contrast in the sample and therefore the extent of lipid exchange[27,28,29,30,31,32,33,34,35]. Notice that the earliest measured R(t) data do not begin at R(t)=1 at 30 °C and 36 °C, indicating that a significant amount of lipid exchange occurred during the first 3 s after mixing, which was not experimentally accessible due to the delay time (t_{delay} = 2.4 s) of the employed stopped-flow mixing protocol. Meanwhile, the measured R(t) at 20 °C remained approximately constant for the first (2-3) minutes. For the lipid exchange kinetics measured at 30 °C and 36 °C, R(t) rapidly decayed to ≈0.5 within 100 s, suggesting the outer leaflet lipids have completely exchanged and equilibrated within minutes. Accordingly, capturing the mβCD-catalyzed lipid exchange was made possible using stopped-flow SANS and would be difficult to capture with manual pipette mixing. Capturing even earlier process time points (t < 3 s) will require a different mixer type with smaller void volume, smaller tubing void volumes, and higher total flow rates to decrease the delay time.

The R(t) continued to decay at longer times as the lipids flip-flop between the inner and outer leaflets. TR-SANS data for the slower flip-flop process (t > 5 min) can be collected with discrete samples mixed by hand and loaded into standard SANS sample cells, as the manual pipette

View Video

s slow enough to be mixed and measured discretely, and this measurement did not

Introduction

mixed by manual pipette mixing. However, kinetic processes on time scales less than minutes will require this stopped-flow mixing and TR-SANS measurement procedure.

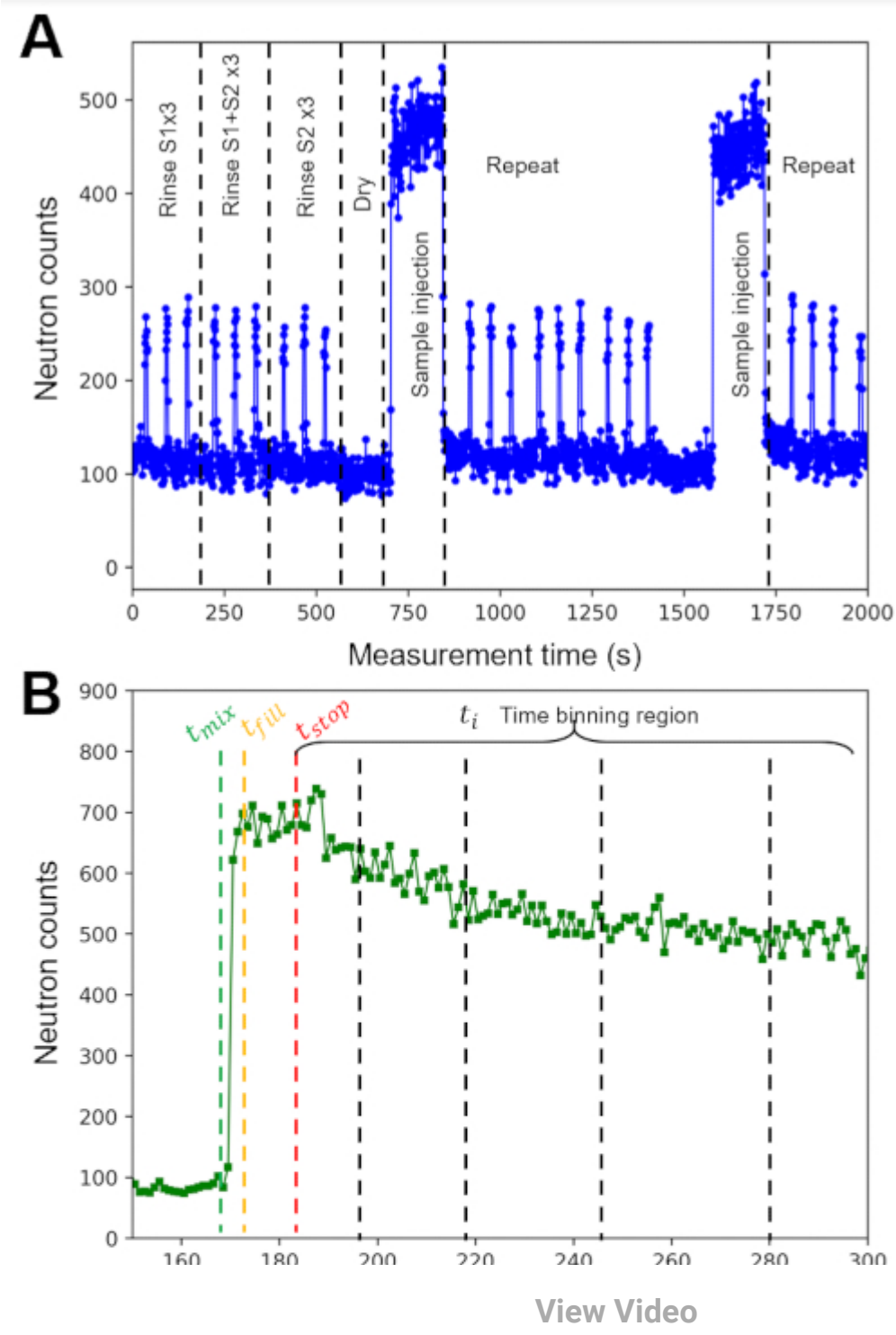

View Video

Introduction

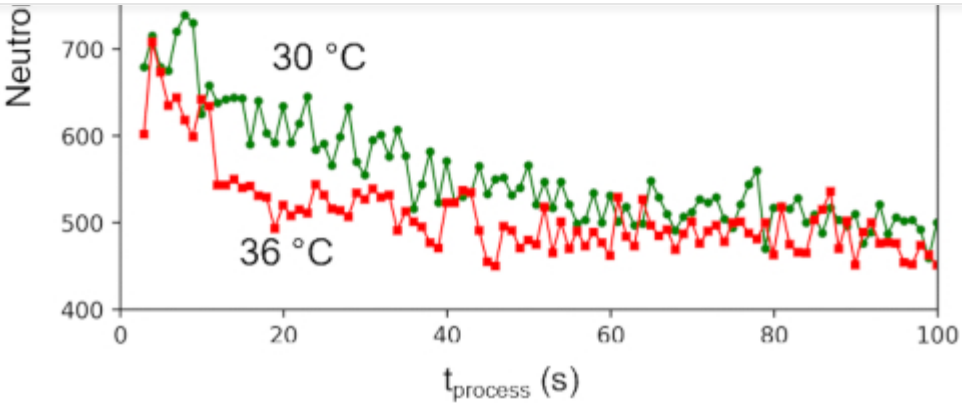

Figure 4: Representative raw neutron count rate data collected throughout mixing and cleaning injection cycles. (**A**) Example of the neutron count rate (middle detector) as a function of time during repeated rinsing sequences, drying sequence, and mixed sample injection sequence over multiple cycles. The sample in (**A**) was a salt buffer background, and the changes in intensity over time reflect the variations in the background count rate, not a change in the sample. (**B**) Monitor-normalized neutron count rate as a function of the experiment time after the injection of mixed H-lipid and D-lipid vesicles at 30 °C. The vertical dashed lines indicate the mixing start time (t_{mix}), the fill time (t_{fill}), the flow stop time (t_{stop}), and time binning region (t_i). The decay in count rate after t_{stop} is due to loss of contrast in the sample as the lipid exchange between vesicles. (**C**) Monitor normalized neutron count rates as a function of exchange process time for the first 100 s of the experiment at (blue) 20 °C, (green) 30 °C, and (red) 36 °C. The event mode data are processed into 1 s bins. Abbreviations: S1 = solvent 1; S2 = solvent 2; t_{mix} = experiment time at which the sample solutions are mixed; t_{fill} = experiment t... at which the sample cell is filled; t_{stop} = experiment time at which the flow is stopped; $t_{process}$ =

View Video

d kinetic process time of interest. **Please click here to view a larger version of this**

Introduction

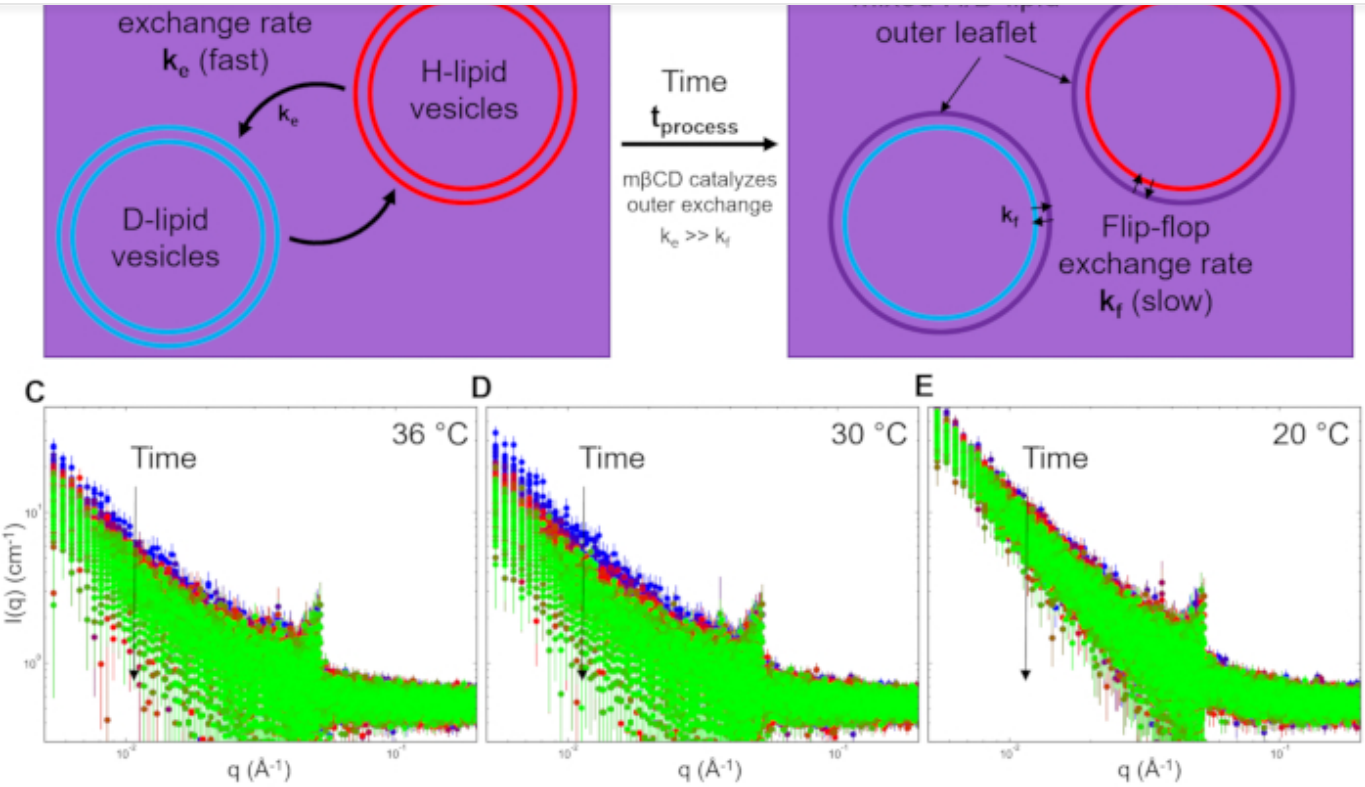

Figure 5: Illustration of catalyzed exchange of the outer layer of lipid vesicles and corresponding changes in the scattered intensity (*I*) as a function of the scattering vector (*q*) at various temperatures. Schematic showing lipid exchange between H-lipid and D-lipid vesicles after (**A**) initial mixing at t = 0 and (**B**) exchange of the outer layer catalyzed by methyl-β-cyclodextrin (mβCD). Reduced neutron scattering intensity as a function of scattering wave vector q. Stopped-flow mixing experiments and VSANS measurements were repeated at (**C**) 36 °C, (**D**) 30 °C, and (**E**) 20 °C. The presented data were binned into 3 s intervals over the first 10 min after mixing at each specified temperature. Error bars are the propagated uncertainty fro... the counting statistics and represent one standard deviation. Abbreviations: k_e = rate consta...

View Video

ange, also referred to as lipid flip-flop; I(q) = measured SANS intensity with units of cm

Introduction

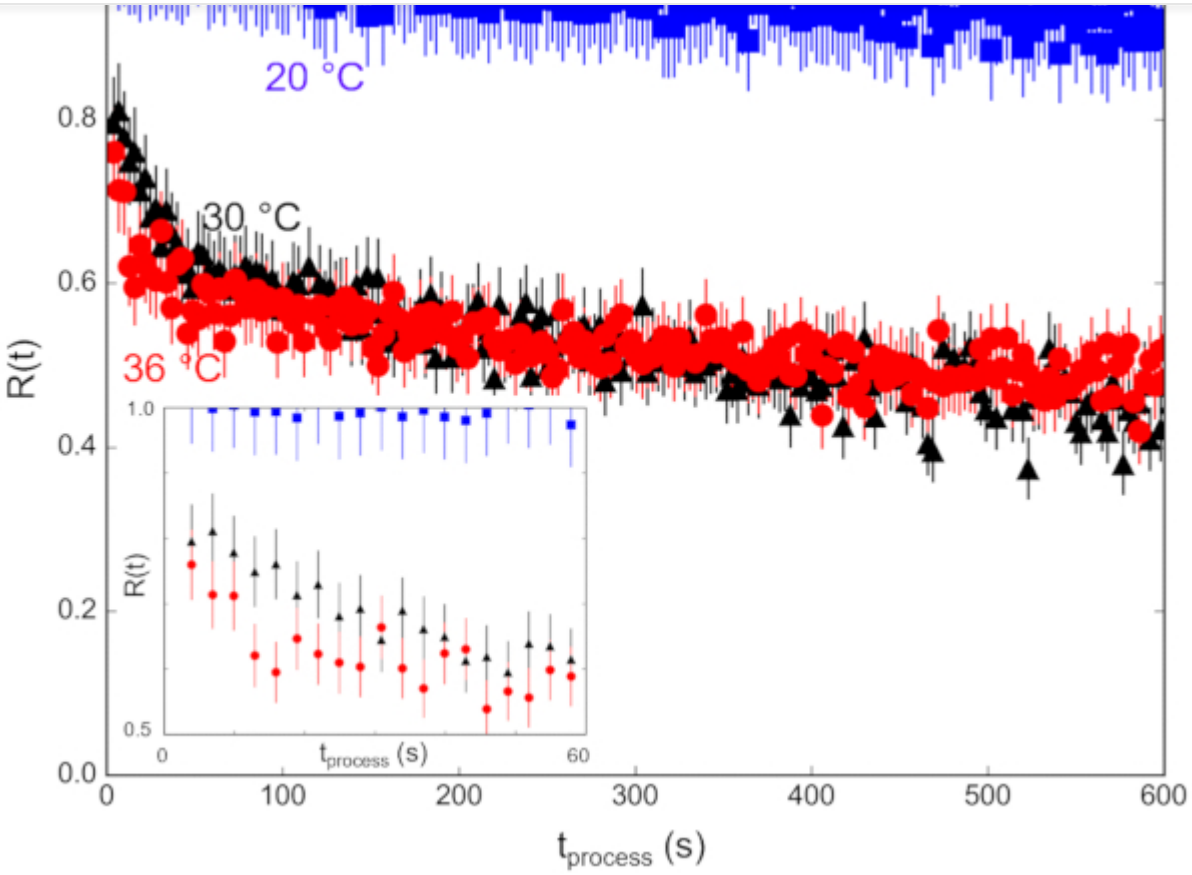

Figure 6: Normalized scattered intensity corresponding to the fraction of lipids exchanged that can be modeled to extract rate constants for the kinetic processes of interest. (**A**) Lipid exchange between the outer leaflet of the vesicles occurring at time scales between 3 s and 600 s measured at (blue) 20 °C, (black) 30 °C, and (red) 36 °C. The inset in the figure zooms in on the first 60 s of the kinetic process. Error bars are the propagated uncertainty from the numerical integration of the scattering intensities and represent one standard deviation. Abbreviations: R(t) = normalized scattered intensity; $t_{process}$ = corrected process tim of interest. **Please click here to view a larger version of this figure.**

View Video

Introduction

where the time scales of interest are ≈1 s to 5 min. For time scales greater than 5 min, manually mixing the samples and loading them into standard scattering cells may be easier and desirable, especially for high-viscosity samples, gels, or pastes. Accessing time scales less than 1 s requires a different mixing apparatus, lower total void volumes, and higher total flow rates to lower the delay time. It is also important to note that studying kinetic processes on these short time scales will likely require repeated sample injections to accumulate sufficient scattering counting statistics on the millisecond time scale with TR-SANS. If total sample volumes are limited, it may be desirable to use a higher flux technique, such as light scattering or X-ray scattering, which requires fewer sample injections or less sample volume per injection, assuming that sufficient scattering contrast exists with light or X-ray scattering.

This modular stopped-flow SANS approach creates several key advantages and disadvantages compared to commercially available stopped-flow instruments that have been optimized for neutron scattering experiments. Key advantages include (1) alternating TR-SANS measurements between different sample cells during rinsing periods to maximize the use of neutron beam time, (2) adapting the number of syringes, syringe volumes, and mixer types for ternary sample mixing or other more complex sample mixing requirements, and (3) allowing for longer measurement periods by isolating the sample cell and eliminating back diffusion at longer time scales (>10 min). Although not implemented here, the modularity of the mixing cell design also would allow for simultaneous data collection with multiple measurement methods, such as combing SA... UV-Vis, and fluorescence measurements[70]. Two key disadvantages of this modular setup

View Video

) relatively longer mixing delay times (1 s to 3 s) compared to other systems that can

Introduction

greater than 30 °C.

Collecting preliminary SANS data on the samples of interest prior to performing *in situ* mixing experiments is important for collecting the best TR-SANS data, particularly in experiments designed to monitor molecular exchange kinetics, such as the example presented here. Determining accurate values of I(0) and I(∞) is critical for calculating accurate values of the normalized intensity, R(t), that is modeled to extract the desired kinetic parameters. The value of I(0) can be directly calculated from the measured scattering intensities of the separate H-vesicle and D-vesicle stocks, and I(∞) can be determined by preparing a separate vesicle sample prepared from a 50/50 mixture of H-lipids/D-lipids. The scattering data from these control samples can also be used to determine the optimal q-range and SANS instrument configuration for the TR-SANS measurement to maximize the signal and verify the progression of exchange kinetics during the TR-SANS experiments. If the measured intensity at the first time point after mixing does not equal the calculated I(0), then faster mixing times may be needed to capture all of the processes of interest. Once the measured intensity has reached I(∞), the exchange process is complete, and the cell can be emptied and cleaned in preparation for the next injection.

To successfully mix liquid sample for TR-SANS, it is critical to ensure that all syringes, valves, and tubing lines are primed and air-free, and that all the tubing connections are secure to prevent leakage. Failing to perform these critical steps correctly could result in inaccurate mixing

View Video

le cell will decrease the measured SANS intensity because of reduced sample volume

Introduction

in the measured scattering intensity over time may indicate poor sample mixing, valve leakage, air bubbles in the sample cell, or sample back-diffusion.

Collecting a transmission measurement for each sample during a TR-SANS experiment is critical for reducing the collected data to an absolute intensity. It is possible to simultaneously collect scattering and transmission data on some SANS instruments, which simplifies the overall TR-SANS data acquisition programming; however, this is not possible on all instruments, including the VSANS instrument used in this protocol. Because the sample transmission and sample scattering measurements required different instrument configurations, transmission measurements were collected at the end of the scattering measurements (protocol step 7.2.4) to ensure that scattering data were measured at the earliest time points after the sample was injected into the cell. The transmission only depends on the total elemental composition, sample path length, and the neutron wavelength. Therefore, the transmission should not change if the total elemental composition remains constant throughout the time-resolved experiment. Large differences in the transmission values between repeated runs of the same sample indicate a problem from either inconsistent mixing sample volumes, incomplete filling of the sample cell, air bubbles, or valve leakage and sample backflow during the experiment.

A unique advantage of TR-SANS is that the measured intensity is dependent on the scattering vector (q) and can be used to probe spatial changes at the nanoscale. When combined with the stopped-flow mixing device, TR-SANS can probe these nanoscale changes on the second to

View Video

ymer and protein aggregation upon excipient addition, nanoparticle growth and decay,

Introduction

more liquid samples. This flexibility enables the systematic investigation of additives on the kinetics of interest. For example, different volumes of a concentrated antimicrobial peptide solution could be mixed with H-vesicle and D-vesicle solutions to study the effects of peptide concentration on lipid exchange kinetics[45,46]. Additionally, because all sealed fluid paths are encased in a temperature-controlled enclosure, which includes the sample syringes, valves, mixers, and tubing, the temperature of the system can be changed to extract the thermodynamic parameters related to the kinetic processes of interest.

Disclosures

The authors have no conflicts of interest to declare.

Acknowledgments

Access to the NG3 VSANS was provided by the Center for High-Resolution Neutron Scattering, a partnership between the National Institute of Standards and Technology and the National Science Foundation under Agreement NO. DMR-2010792. M.H.L.N acknowledges the funding provided by Mitacs Globalink (Canada). The identification of any commercial products or trade names is to foster understanding and does not imply endorsement or recommendation by the National Institute of Standards and Technology.

Materials

View Video

	Instruments		0.15 mL dead volume (larger dead volume available)
tubing	IDEX Health & Science	1507L	PFA Tubing Natural 1/16 inch OD x 0.040 inch ID x 50 ft

Introduction

valves			10-32 coned threaded ports, USB universal actuator
High-pressure switch valves	Vici Valco	C82X-1574EUHB	Vici 4 port switch valves, 15000 psi max, 0.25 mm bore, 1/16 inch OD tubing, 10-32 coned threaded ports, USB universal actuator
High-pressure syringes	Cetoni	A2019000358	3 mL stainless steel syringe, 510 bar max, 21 mL/min flow rate max
Low-pressure flow selector valves	Vici Valco	C25-3180EUHB	Vici 10 position selector valves, max 250 psi liquid, 0.75 mm bore, 1/16 inch OD tubing, 1/4-28 threaded ports, USB universal actuator
neMESYS high-pressure syringe pumps	Cetoni	A3921000103	Max force 2600 N
neMESYS mid-pressure syringe pumps	Cetoni	A3921000131	Max force 1000 N
Power supply	Cetoni	A3921000127	Base 600, supplies power for up to 4 high pressure pumps
Quartz flow-through sample cell	Starna Scientific	3-2.30-Q-1/TC	Quartz micro flow cells, 2 mm path length (1 mm available), 2 mm by 2 mm by 30 mm internal dimension
Quartz windows	Technical Glass Products	NA	GE 124 Clear fused quartz ground and polished plates, 11.75 inch by 23.75 inch by 0.375 inch thick
Stainless steel 10-32 coned compression fittings	IDEX Health & Science	U-321X, U-320X	316 stainless steel ferrule (U-321X) and nut (U-320X) -Valco type, 10-32 coned, for 1/16 inch OD stainless steel tubing
Stainless steel tubing	IDEX Health & Science	U-102	Stainless Steel Tubing 1/16 inch OD x 0.020 inch ID, 10 cm, various precut lengths available
Syringe pump control software	Cetoni	T6000000004	QmixElements software for nemesys pumps, QmixSDK software development kit
Thermoelectric air conditioner	EIC Solutions	AAC-140C-4XT-HC	Thermoelectric air conditioner mounted on insulated enclosure to control the pump, valve, mixer, and sample temperature
T-slot railing	McMaster-Carr	47065T103	Aluminum t-slotted railing (1.5 inch by 1.5 inch) cut to various lengths
Vapor locking bottle caps	Cole-Parmer	EW-12018-02	Four 304 SS port inserts, 1/4"-28 threads, GL45 bottle cap size, PTFE body, SS threads, PP collar

DOWNLOAD MATERIALS LIST

References

1. Melnichenko, Y. B., Wignall, G. D. Small-angle neutron scattering in materials science: Recent practical applications. *Journal of Applied Physics*. **102**, (2), 021101 (2007).
2. Grillo, I. Small-angle neutron scattering and applications in soft condensed matter. *Soft Matter Characterization*. Borsali, R., Pecora, R. Springer. Dordrecht. (2008).
3. Hollamby, M. J. Practical applications of small-angle neutron scattering. *Physical*

View Video

ch, V., Fu, Z. KWS-3: Very small angle diffractor with focusing mirror. *Journal of large-*

6. Gilbert, P. H., *et al.* Preservative induced polysorbate 80 micelle aggregation. *Journal of Pharmaceutical Sciences*. **10**, (6), 2395-2404 (2021).
7. Terashima, T., *et al.* In situ and time-resolved small-angle neutron scattering observation of star polymer formation via arm-linking reaction in ruthenium-catalyzed living radical polymerization. *Macromolecules*. **43**, (19), 8218-8232 (2010).
8. Hashimoto, K., Fujii, K., Nishi, K., Shibayama, M. Ion gel network formation in an ionic liquid studied by time-resolved small-angle neutron scattering. *The Journal of Physical Chemistry B*. **122**, (40), 9419-9424 (2018).
9. Conn, C. E., *et al.* Membrane protein structures in lipid bilayers; small-Angle neutron scattering with contrast-matched bicontinuous cubic phases. *Frontiers in Chemistry*. **8**, 619470 (2021).
10. van't Hag, L., *et al.* Protein-eye view of the in meso crystallization mechanism. *Langmuir*. **35**, (25), 8344-8356 (2019).
11. Mahieu, E., *et al.* Observing protein degradation by the PAN-20S proteasome by time-resolved neutron scattering. *Biophysical Journal*. **119**, (2), 375-388 (2020).
12. Ibrahim, Z., *et al.* Time-resolved neutron scattering provides new insight into protein substrate processing by a AAA+ unfoldase. *Scientific Reports*. **7**, (1), 40948 (2017).
13. Hollamby, M. J., *et al.* Growth of mesoporous silica nanoparticles monitored by time-resolved small-angle neutron scattering. *Langmuir*. **28**, (9), 4425-4433 (2012).
14. Blin, J. L., Impéror-Clerc, M. Mechanism of self-assembly in the synthesis of silica mesoporous materials: in situ studies by X-ray and neutron scattering. *Chemical Society Reviews*. **42**, (9), 4071-4082 (2013).
15. Impéror-Clerc, M., Grillo, I., Khodakov, A. Y., Durand, D., Zholobenko, V. L. New insights int

View Video

ttering investigation. *Chemical Communications*. **8**, 834-836 (2007).

Introduction

dynamics. *The Journal of Physical Chemistry Letters*. **4**, (11), 1959-1964 (2013).

18. Amann, M., *et al.* Kinetic pathways for polyelectrolyte coacervate micelle formation revealed by time-resolved synchrotron SAXS. *Macromolecules*. **52**, (21), 8227 (2019).
19. Varga, Z., Wacha, A., Bóta, A. Osmotic shrinkage of sterically stabilized liposomes as revealed by time-resolved small-angle X-ray scattering. *Journal of Applied Crystallography*. **47**, (1), 35-40 (2014).
20. Panine, P., Finet, S., Weiss, T. M., Narayanan, T. Probing fast kinetics in complex fluids by combined rapid mixing and small-angle X-ray scattering. *Advances in Colloid and Interface Science*. **127**, (1), 9-18 (2006).
21. Grillo, I. Applications of stopped-flow in SAXS and SANS. *Current Opinion in Colloid & Interface Science*. **14**, (6), 402-408 (2009).
22. Gomez-Hens, A., Perez-Bendito, D. The stopped-flow technique in analytical chemistry. *Analytica Chimica Acta*. **242**, 147-177 (1991).
23. Patel, J. T., Belsham, H. R., Rathbone, A. J., Friel, C. T. Use of stopped-flow fluorescence and labeled nucleotides to analyze the ATP turnover cycle of kinesins. *Journal of Visualized Experiments: JoVE*. (92), e52142 (2014).
24. Biro, F. N., Zhai, J., Doucette, C. W., Hingorani, M. M. Application of stopped-flow kinetics methods to investigate the mechanism of action of a DNA repair protein. *Journal of Visualized Experiments: JoVE*. (37), e1874 (2010).
25. Raney, K. D., Sowers, L. C., Millar, D. P., Benkovic, S. J. A fluorescence-based assay for monitoring helicase activity. *Proceedings of the National Academy of Sciences of the United States of America*. **91**, (14), 6644-6648 (1994).
26. Roder, H., Maki, K., Cheng, H. Early events in protein folding explored by rapid mixing

View Video

ɔn, A., *et al.* Osmotic swelling of unilamellar vesicles by the stopped-flow light

Introduction

28. Gast, K., Nöppert, A., Müller-Frohne, M., Zirwer, D., Damaschun, G. Stopped-flow dynamic light scattering as a method to monitor compaction during protein folding. *European Biophysics Journal*. **25**, (3), 211-219 (1997).
29. Antoun, A., Pavlov, M. Y., Tenson, T., Ehrenberg, M. M. Ribosome formation from subunits studied by stopped-flow and Rayleigh light scattering. *Biological Procedures Online*. **6**, 35-54 (2004).
30. Zhu, Z., Armes, S. P., Liu, S. pH-Induced micellization kinetics of ABC triblock copolymers measured by stopped-flow light scattering. *Macromolecules*. **38**, (23), 9803-9812 (2005).
31. Ye, J., *et al.* Comparative study of temperature-induced association of cyclic and linear poly(N-isopropylacrylamide) chains in dilute solutions by laser light scattering and stopped-flow temperature jump. *Macromolecules*. **41**, (12), 4416-4422 (2008).
32. Liu, X., *et al.* Early stage kinetics of polyelectrolyte complex coacervation monitored through stopped-flow light scattering. *Soft Matter*. **12**, (44), 9030-9038 (2016).
33. Garman, E. F., Weik, M. X-ray radiation damage to biological samples: recent progress. *Journal of Synchrotron Radiation*. **26**, (4), 907-911 (2019).
34. Garg, S., Porcar, L., Woodka, A. C., Butler, P. D., Perez-Salas, U. Noninvasive neutron scattering measurements reveal slower cholesterol transport in model lipid membranes. *Biophysical Journal*. **101**, (2), 370-377 (2011).
35. Marquardt, D., *et al.* 1H NMR shows slow phospholipid flip-flop in gel and fluid bilayers. *Langmuir*. **33**, (15), 3731-3741 (2017).
36. Egelhaaf, S. U., Olsson, U., Schurtenberger, P. Time-resolved SANS for surfactant phase transitions. *Physica B: Condensed Matter*. **276-278**, 326-329 (2000).
37. Tabor, R. F., Eastoe, J., Grillo, I. Time-resolved small-angle neutron scattering as a lamell

View Video

dzielski, M., Bergmeier, M., Hoffmann, H., Müller, M., Grillo, I. Vesicle gel formed by a

Introduction

water emulsions through contrast variation time-resolved small-sngle neutron scattering. *Langmuir*. **35**, (47), 15204-15213 (2019).

40. Lee, Y. -T., Pozzo, L. D. Contrast-variation time-resolved small-angle neutron scattering analysis of oil-exchange kinetics between oil-in-water emulsions stabilized by anionic surfactants. *Langmuir*. **35**, (47), 15192-15203 (2019).
41. Roger, K., Olsson, U., Schweins, R., Cabane, B. Emulsion ripening through molecular exchange at droplet contacts. *Angewandte Chemie International Edition*. **54**, (5), 1452-1455 (2015).
42. Nakano, M., Fukuda, M., Kudo, T., Endo, H., Handa, T. Determination of Interbilayer and Transbilayer Lipid Transfers by Time-Resolved Small-Angle Neutron Scattering. *Physical Review Letters*. **98**, (23), 238101 (2007).
43. Nakano, M., *et al.* Flip-flop of phospholipids in vesicles: kinetic analysis with time-resolved small-angle neutron scattering. *The Journal of Physical Chemistry B*. **113**, (19), 6745-6748 (2009).
44. Nguyen, M. H. L., *et al.* Methanol accelerates DMPC flip-flop and transfer: A SANS study on lipid dynamics. *Biophysical Journal*. **116**, (5), 755-759 (2019).
45. Nguyen, M. H. L., *et al.* Peptide-induced Lipid flip-flop in asymmetric liposomes measured by small angle neutron scattering. *Langmuir*. **35**, (36), 11735-11744 (2019).
46. Nguyen, M. H. L., *et al.* Time-resolved SANS reveals pore-forming peptides cause rapid lipid reorganization. *New Journal of Chemistry*. **45**, (1), 447-456 (2021).
47. Xia, Y., *et al.* Effects of nanoparticle morphology and acyl chain length on spontaneous lipid transfer rates. *Langmuir*. **31**, (47), 12920-12928 (2015).
48. Xia, Y., *et al.* Morphology-induced defects enhance lipid transfer rates. *Langmuir*. **32**, (38),

View Video

ic, S., *et al.* Time-resolved small-angle neutron scattering as a probe for the dynamics

for the mode of action: How natural antimicrobial peptides affect lipid transport. *Journal of Colloid and Interface Science*. **582**, 793-802 (2021).

51. Willner, L., Poppe, A., Allgaier, J., Mokenbusch, M., Richter, D. TIme-resolved SANS for the determintioan of unimer exchange kinetics in block copolymer micelles. *Europhysics Letters*. **55**, (5), 667 (2001).
52. Lund, R., Willner, L., Stellbrink, J., Lindner, P., Richter, D. Logarithmic chain-exchange kinetics of diblock copolymer micelles. *Physical Review Letters*. **96**, (6), 068302 (2006).
53. Lund, R., Willner, L., Richter, D., Dormidontova, E. E. Equilibrium chain exchange kinetics of diblock copolymer micelles: Tuning and logarithmic relaxation. *Macromolecules*. **39**, (13), 4566-4575 (2006).
54. Lund, R., Willner, L., Richter, D. Kinetics of block copolymer micelles studied by small-angle scattering methods. in Controlled Polymerization and Polymeric Structures. *Advances in Polymer Science*. Abe, A., Lee, K. S., Leibler, L., Kobayashi, S. Springer. Cham. 51 (2013).
55. Choi, S. -H., Lodge, T. P., Bates, F. S. Mechanism of molecular exchange in diblock copolymer micelles: hypersensitivity to core chain length. *Physical Review Letters*. **104**, (4), 047802 (2010).
56. Choi, S. -H., Bates, F. S., Lodge, T. P. Molecular exchange in ordered diblock copolymer micelles. *Macromolecules*. **44**, (9), 3594-3604 (2011).
57. Lu, J., Bates, F. S., Lodge, T. P. Chain exchange in binary copolymer micelles at equilibrium: confirmation of the independent chain hypothesis. *ACS Macro Letters*. **2**, (5), 451-455 (2013).
58. Lu, J., Bates, F. S., Lodge, T. P. Remarkable effect of molecular architecture on chain exchange in triblock copolymer micelles. *Macromolecules*. **48**, (8), 2667-2676 (2015).

View Video

ey, E. G., *et al.* Size evolution of highly amphiphilic macromolecular solution assemblies

Macro Letters. **3**, (11), 1106-1111 (2014).

61. Schantz, A. B., *et al.* PEE-PEO block copolymer exchange rate between mixed micelles is detergent and temperature activated. *Macromolecules*. **50**, (6), 2484-2494 (2017).
62. Lantz, K. A., *et al.* Cavitation enables switchable and rapid block polymer exchange under high-χN conditions. *Macromolecules*. **51**, (17), 6967-6975 (2018).
63. Murphy, R. P., *et al.* Capillary RheoSANS: measuring the rheology and nanostructure of complex fluids at high shear rates. *Soft Matter*. **16**, (27), 6285-6293 (2020).
64. Stopped Flow Sans. *usnistgov*. Available from: https://github.com/usnistgov/stopped-flow-sans (2021).
65. Kline, S. Reduction and analysis of SANS and USANS data using IGOR Pro. *Journal of Applied Crystallography*. **39**, (6), 895-900 (2006).
66. Doktorova, M., *et al.* Preparation of asymmetric phospholipid vesicles for use as cell membrane models. *Nature Protocols*. **13**, (9), 2086-2101 (2018).
67. Huang, Z., London, E. Effect of cyclodextrin and membrane lipid structure upon cyclodextrin-lipid interaction. *Langmuir*. **29**, (47), 14631-14638 (2013).
68. Sugiura, T., Ikeda, K., Nakano, M. Kinetic analysis of the methyl-β-cyclodextrin-mediated intervesicular transfer of pyrene-labeled phospholipids. *Langmuir*. **32**, (51), 13697-13705 (2016).
69. Scott, H. L., *et al.* On the mechanism of bilayer separation by extrusion, or why your LUVs are not really unilamellar. *Biophysical Journal*. **117**, (8), 1381-1386 (2019).
70. Dicko, C., *et al.* NUrF-Optimization of in situ UV-vis and fluorescence and autonomous characterization techniques with small-angle neutron scattering instrumentation. *Revie Scientific Instruments*. **91**, (7), 075111 (2020).

View Video

Introduction

Copyright © 2022 MyJoVE Corporation. All rights reserved

View Video